Contrasting carrier doping effects in the Kondo insulator $CeOs_2Al_{10}$: The influential role of c-f hybridization in spin-gap formation

A. Bhattacharyya,[1,2,*] D. T. Adroja,[1,2,†] A. M. Strydom,[2] J. Kawabata,[3] T. Takabatake,[3] A. D. Hillier,[1] V. Garcia Sakai,[1] J. W. Taylor,[1] and R. I. Smith[1]

[1]*ISIS Facility, Rutherford Appleton Laboratory, Chilton, Didcot, Oxon OX11 0QX, United Kingdom*

[2]*Highly Correlated Matter Research Group, Physics Department, University of Johannesburg, Auckland Park 2006, South Africa*

[3]*Department of Quantum Matter, ADSM and IAMR, Hiroshima University, Higashi-Hiroshima 739-8530, Japan*

(Received 4 July 2014; revised manuscript received 30 October 2014; published 17 November 2014)

The effects of electron (Ir) and hole (Re) doping on the hybridization gap and antiferromagnetic order have been studied by magnetization, muon spin relaxation (μ^+SR), and inelastic neutron scattering on polycrystalline samples of $Ce(Os_{1-x}Ir_x)_2Al_{10}$ ($x = 0.08$ and 0.15) and $Ce(Os_{1-y}Re_y)_2Al_{10}$ ($y = 0.03$). μ^+SR spectra clearly reveal bulk magnetic ordering below 20 and 10 K for $x = 0.08$ and 0.15 samples, respectively, with heavily damped oscillations of the muon asymmetry. Our important findings are that a small amount of electron doping (i) completely suppresses the inelastic magnetic excitations at low temperatures, which were observed at 11 meV in the undoped compound, and the magnetic response transforms into a broad quasielastic response, and (ii) surprisingly, the internal field at the corresponding muon site is remarkably enhanced by an order of magnitude compared with the parent compound. Moreover, a small amount (3% Re) of hole doping results in a significant reduction of the intensity of 11 meV peak and an increased c-f hybridization, which is in agreement with the reduction of the Ce ordered moment seen through neutron diffraction and μ^+SR. The main origin of the observed doping effect is an extra $5d$ electron being carried by Ir and a hole carried by Re with respect to the Os atom. The absence of a spin gap/spin wave, despite a larger ordered state moment of Ce, in the electron-doped system cannot be explained based on a conventional theory of magnetism. Thus, the obtained results demonstrate a great sensitivity to the carrier doping and provide additional ways to study the anomalous magnetic properties in the CeT_2Al_{10} (T = Fe, Ru, and Os).

DOI: 10.1103/PhysRevB.90.174422 PACS number(s): 71.27.+a, 75.20.Hr, 76.75.+i, 25.40.Fq

I. INTRODUCTION

Yb- or Ce-based compounds having elements with f electrons display a rich variety of properties, including an enormous increase of the quasiparticle effective mass [heavy fermion (HF) system], a Kondo insulating state, and unconventional superconductivity [1–3]. Over the last two decades, these properties have attracted considerable interest in condensed-matter physics. The qualitative representation of both HF and the Kondo insulating state is based on the knowledge that the ground state is a consequence of the competition between Kondo and Ruderman-Kittel-Kasuya-Yosida (RKKY) interactions [4]. If the RKKY interaction dominates, the system orders magnetically. However, if the Kondo interaction dominates, theory predicts that a hybridization between the localized f electron and the conduction carrier states should lead to the opening of a charge/spin gap (or pseudogap) at the Fermi energy [5–9]. Though this picture is not in dispute, the well-defined predictions of the hybridization scenario have so far escaped direct experimental verification. One of the key predictions is a simple scaling relationship between the magnitude of the direct energy gap, Δ, in the excitation spectrum and the enhancement of the effective mass of charge carriers, $m^\star$, in the coherent regime [10]. Several HF materials, such as $CeAl_3$ [11], show no evidence of such a gap, whereas in the prototypical compounds such as UPt_3 and URu_2Si_2, the gap is attributed to a magnetic ground state [12–14].

Caged-type Ce-based compounds with the general formula CeT_2Al_{10} (T = Fe, Ru, and Os) have attracted considerable attention due to the Kondo semiconducting paramagnetic ground state (down to 40 mK) observed in $CeFe_2Al_{10}$ and anomalously high antiferromagnetic (AFM) ordering temperature with a spin-gap formation at low temperatures in Kondo semimetal $CeRu_2Al_{10}$ and Kondo semiconductor $CeOs_2Al_{10}$ [15–20]. AFM ordering temperature of these Ce compounds is found to be higher than that of the Gd compounds, which rules out that the magnetic order is caused by simple RKKY interactions. According to the de Gennes scaling, T_N (Néel temperature) for a Gd compound is expected to be 100 times that for the Ce counterpart if we neglect the crystal-field effect and possible differences in the Fermi surface. Charge-density-wave-like instability is found in optical conductivity measurements for CeT_2Al_{10} (T = Ru, Os), which develops along the b axis at temperatures slightly higher than T_N. It was suggested that this electronic instability induces AFM order [21]. The formation of long-range magnetic ordering from the Kondo semiconducting/semimetallic state itself is unexpected and these are examples of this mysterious coexistence of electronic ground states. These compounds also reveal robust anisotropy in magnetic and transport properties, which has been elucidated on the basis of single-ion crystal electric-field anisotropy in the presence of strongly anisotropic hybridization between the localized $4f$ electron and the conduction electrons. Recently, Kawabata *et al.* [22] suggested that the suppression of T_N is correlated with the gap energy Δ which is a function of the amount of electron/hole doping [23]. They therefore concluded that the presence of the hybridization gap is necessary for the AFM order at unusually high T_N in $CeOs_2Al_{10}$. Therefore, it is

*amitava.bhattacharyya@stfc.ac.uk
†devashibhai.adroja@stfc.ac.uk

important to confirm whether this interesting conclusion of the hybridization is correct. A direct method for measuring the gap is inelastic neutron scattering (INS), and muon spin relaxation (μ^+SR) can ensure that we have seen bulk magnetic order rather than clusters of magnetism from an inhomogeneous sample.

In this paper, we report the properties of doping of $5d$ electrons (Ir) and holes (Re) on the Kondo semiconductor $CeOs_2Al_{10}$ by measuring magnetization, muon spin relaxation, and inelastic neutron scattering on the polycrystalline samples of $Ce(Os_{1-x}Ir_x)_2Al_{10}$ ($x = 0.08$ and 0.15) and $Ce(Os_{1-y}Re_y)_2Al_{10}$ ($y = 0.03$). The broad maxima at around 45 K in magnetic susceptibility for the undoped sample changes to the Curie-Weiss behavior of Ce^{3+} with increasing electron doping. This change means that doping of $5d$ electrons localizes the $4f$ electron state in $CeOs_2Al_{10}$. With hole doping, the broad maximum of magnetic susceptibility initially (up to $y = 0.05$) remains nearly at the same temperature and then disappears (at $y = 0.1$) [22]. The spin-flop transition in M-H for the Ir substituted samples revealed that the direction of the ordered moment changes from the c axis to the a axis with increasing x to 0.15. In spite of the significant increase of magnetic moment from 0.29 μ_B for $x = 0$ to 0.92(3) μ_B for $x = 0.08$ per Ce atom [24,25], T_N decreases gradually from 28.5 to 7.0 K for $x = 0$ and 0.15, respectively. By the Re substitution (or hole doping), T_N decreases much faster than the electron-doped samples [22].

II. EXPERIMENTAL DETAILS

Polycrystalline samples of $Ce(Os_{1-x}Ir_x)_2Al_{10}$ ($x = 0.08$ and 0.15) and $Ce(Os_{1-y}Re_y)_2Al_{10}$ ($y = 0.03$) were prepared by arc melting of the constituent elements (Ce: 99.99%; Os: 99.99%; Ir: 99.99%; Re: 99.99%; Al: 99.999%) in an argon atmosphere on a water-cooled copper hearth. After being flipped and remelted several times, the boules were wrapped in tantalum foil and annealed at 1123 K for 168 hr under a dynamic vacuum of better than 10^{-6} Torr. Powder x-ray diffraction measurements were carried out using a Panalytical X-Pert Pro diffractometer. Magnetic susceptibility measurements were made using a Quantum Design SQUID magnetometer.

Inelastic neutron-scattering and muon spin relaxation experiments were carried out at the ISIS Pulsed Neutron and Muon Facility of the Rutherford Appleton Laboratory, United Kingdom. In addition, to check the phase purity of the samples, neutron-diffraction measurements were carried out using the General Materials (GEM) time-of-flight (TOF) diffractometer at ISIS. Powders were loaded into 6-mm-diameter cylindrical vanadium sample cans and data were collected at room temperature for between 30–60 minutes per sample. Inelastic neutron-scattering experiments have been performed on the time-of-flight direct geometry chopper spectrometers MARI and MERLIN at the ISIS pulsed neutron facility, United Kingdom. The low-energy, high-resolution, inelastic neutron-scattering measurements were also carried out at the ISIS facility using the indirect geometry TOF high-resolution spectrometers OSIRIS and IRIS with a pyrolytic graphite (PG) (002) analyzer. The INS measurements were carried out between 5 and 100 K [for the $Ce(Os_{0.85}Ir_{0.15})_2Al_{10}$ sample, we measured down to 2 K on MARI]. The powder samples were wrapped in a thin Al foil and mounted inside a thin-walled cylindrical Al can, which was cooled down to 4.5 K inside a top-loading closed-cycle refrigerator with He-exchange gas around the samples. Incident energies of 6, 25, and 100 meV were used on MARI selected via a Gd-Fermi chopper. The μ^+SR measurements were carried out on the MUSR spectrometer with the detectors in the longitudinal configuration. The powdered samples were mounted on a high-purity silver plate using diluted GE varnish and covered with a Kapton film which was cooled down to 1.2 K in a standard He-4 cryostat with He-exchange gas. Spin-polarized muon pulses were implanted into the sample and the positrons from the resulting decay were collected in positions either forward or backward of the initial muon spin direction. The asymmetry of the muon decay is calculated by $G_z(t) = [N_F(t) - \alpha N_B(t)]/[N_F(t) + \alpha N_B(t)]$, where $N_B(t)$ and $N_F(t)$ are the number of counts at the detectors in the forward and backward positions, and α is a constant determined from calibration measurements made in the paramagnetic state with a small (20 G) applied transverse magnetic field.

III. STRUCTURE AND MAGNETIZATION

Room-temperature neutron diffraction study was carried out using the GEM diffractometer. Rietveld crystal structure refinement using the neutron-diffraction data (not shown here) confirmed that the compounds crystallize in the orthorhombic $YbFe_2Al_{10}$-type structure (space group $Cmcm$, No. 63). In this caged-type structure, the Ce atom is surrounded by a polyhedron formed by 4 Os/Ir and 16 Al atoms and forms a zigzag chain along the orthorhombic c axis [25,26]. The refined lattice parameters and unit cell volume are given in Table I. It is clear from neutron-diffraction refinement that a small amount of electron or hole doping does not change lattice parameters and volume drastically. However, for hole doping, the ordered moment is substantially reduced [0.18(1) μ_B], while preserving the anomalous magnetic moment direction along the c axis the same as the $CeOs_2Al_{10}$ compound. On the other hand, for electron doping, the moment orients along the a direction, with the ordered value being 0.92(1) μ_B [25,26].

The temperature (T) variation of the magnetic susceptibility ($\chi = M/H$, where H is the applied magnetic field) measured in zero-field cooled condition with $H = 50$ kOe is shown in Fig. 1(a). $\chi(T)$ shows a drop below 20 and 8 K for $x = 0.08$ and 0.15 samples, respectively with decreasing temperature. This corresponds to the paramagnetic to antiferromagnetic

TABLE I. Lattice parameters of $Ce(Os_{1-x}Ir_x)_2Al_{10}$ for $x = 0$, 0.08, 0.15 and $Ce(Os_{1-y}Re_y)_2Al_{10}$ ($y = 0.03$) refined from the neutron-diffraction data collected at room temperature in the orthorhombic $Cmcm$ space group.

Compounds	a (Å)	b (Å)	c (Å)	V (Å)^3
$x = 0.0$	9.1221	10.2545	9.1694	857.729
$x = 0.08$	9.1193	10.2554	9.1657	857.195
$x = 0.15$	9.1113	10.2544	9.1643	856.229
$y = 0.03$	9.1217	10.2546	9.1704	857.794

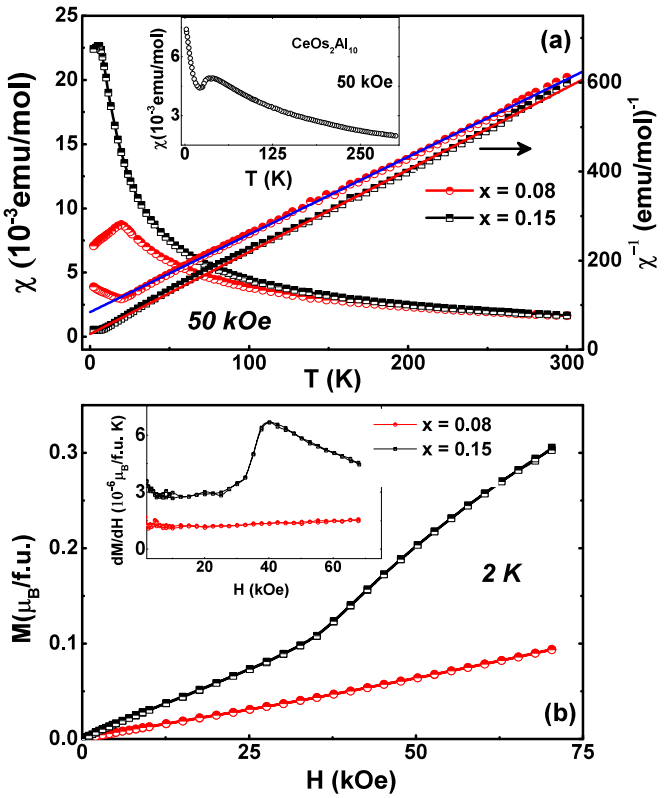

FIG. 1. (Color online) (a) Temperature dependence of dc susceptibility $\chi(T)$ and the inverse $\chi(T)$ of $Ce(Os_{1-x}Ir_x)_2Al_{10}$ [$x = 0$ (inset), 0.08 and 0.15] in an applied magnetic field of 50 kOe. (b) Isothermal field dependence of magnetization at 2 K. Inset: The first derivative of the magnetization with field (dM/dH) vs H at 2 K.

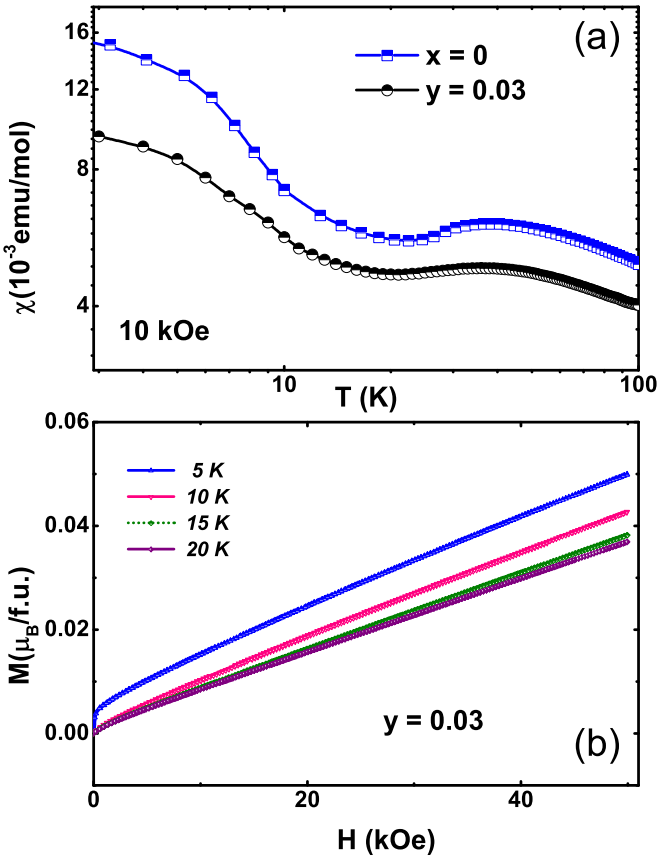

FIG. 2. (Color online) (a) Temperature-dependent magnetic susceptibility $\chi(T)$ of $Ce(Os_{1-y}Re_y)_2Al_{10}$ ($y = 0.0, 0.03$) in an applied magnetic field of 10 kOe. (b) M vs H isotherms at various temperatures for $y = 0.03$.

(PM-AFM) transition in the sample. The magnetic susceptibility of $Ce(Os_{1-x}Ir_x)_2Al_{10}$ ($x = 0.08$ and 0.15) exhibits Curie-Weiss behavior above 100 K. A linear least-squares fit yields an effective magnetic moment $p_{\text{eff}} = 2.15$ and 2.10 μ_B for the two compositions, respectively, which is smaller than the free Ce^{3+}-ion value (2.54 μ_B), and a negative paramagnetic Curie temperature $\theta_p = -48$ and -18 K for $x = 0.08$ and 0.15 samples, respectively. The value of the magnetic moment suggests that the Ce atoms are in their normal Ce^{3+} valence state. A negative value of θ_p is indicative of a negative exchange constant.

Figure 1(b) shows the M versus H isotherms recorded at 2 K for $x = 0.08$ and 0.15. M-H data imply that the net magnetization in the ordered state of $Ce(Os_{1-x}Ir_x)_2Al_{10}$ is extremely low. It is far from saturation as that expected theoretically is $gJ = 2.14\ \mu_B$ for Ce^{3+} ions. This is consistent with the previously reported results [22]. The low values of the observed magnetization are expected for an AFM ground state due to the cancellation of magnetization from different magnetic sublattices of the Ce ions. A clear signature of a field-induced transition is observed for $Ce(Os_{0.85}Ir_{0.15})_2Al_{10}$, as shown in the inset of Fig. 1(b), which warrants further investigation.

$\chi(T)$ data of $Ce(Os_{0.97}Re_{0.03})_2Al_{10}$ are shown in Fig. 2(a), which show a PM-AFM transition below $T_N = 21$ K that matches well with previously reported data [26]. Figure 2(b) shows the M versus H isotherms recorded at different constant temperatures below and above magnetic transition temperature. The M-H data do not show any spin-flip transition like the Ir-doped sample. The ordered moments are substantially reduced but preserve the anomalous direction along the c axis. Neutron-diffraction results suggest a long-range AFM ordering of the Ce sublattice, with a substantially reduced value of the magnetic moment 0.18(1) μ_B for 3% Re doped and 0.92(3) μ_B for 8% Ir doped, occurs below T_N [26]. A list of studied samples and their transitions temperatures is given in Table II.

TABLE II. A list of samples studied for $Ce(Os_{1-x}Ir_x)_2Al_{10}$ ($x = 0, 0.08, 0.15$) and $Ce(Os_{1-y}Re_y)_2Al_{10}$ ($y = 0.03$) and their transition temperatures (T_N = antiferromagnetic ordering temperature), ground-state magnetic moment (μ_{AF}) value, and moment directions obtained from the neutron-diffraction study.

Compounds	T_N (K)	μ_{AF} (μ_B)	moment direction
$x = 0.0$	28.5	0.29(1)	c axis [16,24]
$x = 0.08$	20	0.92(3)	a axis [25]
$x = 0.15$	8		
$y = 0.03$	21	0.18(1)	c axis [26]

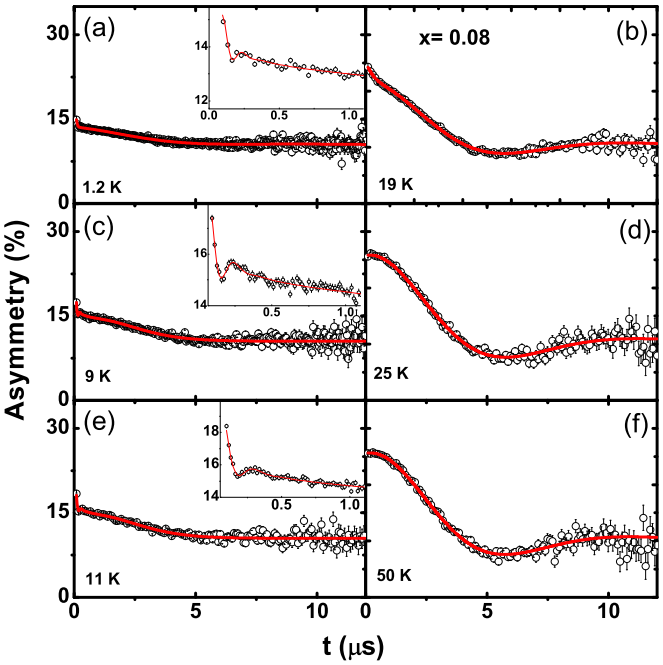

FIG. 3. (Color online) Zero-field muon spin relaxation spectra at various temperatures of $Ce(Os_{1-x}Ir_x)_2Al_{10}$ ($x = 0.08$). The solid lines are least-squares fit to the data as described in the text. Insets: The asymmetry spectra in the short-time region.

IV. MUON SPIN RELAXATION

In order to study the dynamics and the internal field at the muon site, we carried out μ^+SR measurements on $Ce(Os_{1-x}Ir_x)_2Al_{10}$ for $x = 0.08$ and 0.15 samples. Detailed μ^+SR investigations on $CeOs_2Al_{10}$ and $Ce(Os_{1-y}Re_y)_2Al_{10}$ ($y = 0.03$) were reported previously [16,26]. Due to the local nature of the muon technique, a μ^+SR study provides information on the volume fraction of different phases as well as different spin dynamic information for multisite systems. For small amounts of the hole-doped (3% Re) compound, we found a Kubo-Toyabe-type behavior above T_N, and, below T_N, its shows a clear signature of oscillation (internal field 70 G at base temperature) due to the very small magnetic moment (0.18 μ_B) [26].

Figures 3(a)–3(f) show the zero-field time-dependence asymmetry spectra at various temperatures below and above magnetic ordering of $Ce(Os_{1-x}Ir_x)_2Al_{10}$ ($x = 0.08$). It is clear from Fig. 3 that a small amount of electron doping drastically changes the time dependence of asymmetry spectra compared with the pure compound. Above 20 K, we observe Kubo-Toyabe-type behavior [26], i.e., a strong damping at shorter time, and the recovery at longer times, arising from a static distribution of the nuclear dipole moment. In the paramagnetic state, i.e., above 20 K, we used the following function to fit our μ^+SR spectra as shown in Figs. 3(d) and 3(f):

$$G_{z_1}^{\mathrm{KT}}(t) = A_2 e^{-\lambda_2 t}\mathrm{KT}(t) + A_{bg}, \qquad (1)$$

where $\mathrm{KT}(t) = \frac{1}{3}[1 + 2(1 - \sigma_{\mathrm{KT}}^2 t^2)e^{(-\frac{\sigma_{\mathrm{KT}}^2 t^2}{2})}]$ is the well-known static Kubo-Toyabe (KT) function. The initial amplitude of the KT decay is A_2, λ_2 is the electronic relaxation rate, and A_{bg} is a constant background arising from muon stopping on the silver sample holder. A_{bg} was estimated from 50 K data and kept fixed for fitting all the other spectra. The nuclear depolarization rate is σ_{KT}, $\sigma_{\mathrm{KT}}/\gamma_\mu = \Delta$ is the local Gaussian field distribution width, and γ_μ is the gyromagnetic ratio of the muon. σ_{KT} was found to be almost temperature independent, with its value equal to 0.29 μs^{-1}. Using a similar σ_{KT} value, Kambe *et al.* [27] have suggested $4a(0,0,0)$ as the muon stopping site in $CeRu_2Al_{10}$, while for $CeOs_2Al_{10}$ [16], the muon stopping site was assigned to the (0.5, 0, 0.25) position. Very recently, Guo *et al.* [28] investigated $Ce(Ru_{1-x}Rh_x)_2Al_{10}$ using μ^+SR, and their dipolar fields calculation supports the (0.5, 0, 0.25) site for the muons.

Our neutron-diffraction result [25] shows that the value of the ordered magnetic moment is 0.92 μ_B/Ce for $Ce(Os_{0.92}Ir_{0.08})_2Al_{10}$, which is substantially bigger compared to the parent compound [0.29 μ_B/Ce observed in the parent compound $CeOs_2Al_{10}$] [24]. In contrast to our undoped compound which shows three frequencies below magnetic ordering, here we observe heavily damped oscillation.

Below 20 K, all spectra are described uniformly by the phenomenological function

$$G_{z_2}(t) = A_1\cos(\omega t + \phi)e^{-\lambda_1 t} + A_3 e^{-\lambda_3 t} + G_{z_1}^{\mathrm{KT}}(t), \qquad (2)$$

where λ_i ($i = 1$ and 3) is the muon depolarization rate (arising from the distribution of the internal field), ϕ is the phase, and $\omega = \gamma_\mu H_{\mathrm{int}}$ is the muon precession frequency (H_{int} is the internal field at the muon site). The first term represents the transverse components of the internal fields seen by the muons along which they precess, while the second term represents the longitudinal component. The last term in Eq. (2) is the Kubo-Toyabe term, which accounts for the dip seen in the μ^+SR spectra near 5.5 μs, even in the magnetically ordered state, indicating that the internal field seen by the muons on this site is smaller than that of the nuclear field. This suggests that the corresponding muon site can be assigned to the $4a$ crystallographic position [28].

The temperature dependencies of these parameters are shown in Figs. 4(a)–4(d). Below 20 K, as shown in Fig. 4(a), there is a loss of initial asymmetry A_2 compare with the high-temperature value. The initial asymmetry associated with frequency term A_1 starts to increase below this temperature (20 K) [see Fig. 4(a)], indicating the onset of a long-range ordered state in $x = 0.08$, which agrees with the specific heat and magnetic susceptibility data [22]. The temperature dependence of Lorentzian decay term λ_2 starts to increase below 20 K. λ_1 associated with the oscillating term almost remains constant. Figure 4(d) shows the temperature dependence of the muon depolarization rate which seems temperature independent. Figure 4(b) shows the temperature dependence of the internal field (or muon precession frequency) at the muon site. This shows that the internal fields appear below 20 K, signifying clear evidence for long-range magnetic order. However, the associated internal fields (approximately 500 G) are found to be one order of magnitude larger than in comparison to the $CeOs_2Al_{10}$ ($H_{\mathrm{int}} = 40$ G at base temperature) compound, which indicates a large ordered state magnetic moment of the Ce^{3+} ion. This observation is in accordance with our recent neutron-diffraction results [25].

Figures 5(a)–5(f) show the zero-field asymmetry spectra for the $Ce(Os_{0.85}Ir_{0.15})_2Al_{10}$ sample. The Kubo-Toyabe behavior

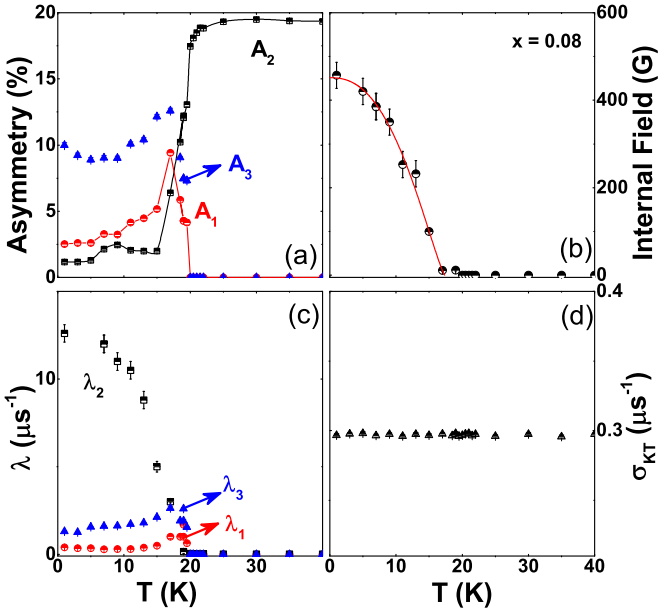

FIG. 4. (Color online) The temperature dependence of (a) the initial asymmetries A_1, A_2, and A_3 and (b) the internal field on the muon site. The solid line in (b) is fit to Eq. (3) (see text). (c),(d) The depolarization rates λ_1, λ_2, λ_3 and σ_{KT} of $Ce(Os_{1-x}Ir_x)_2Al_{10}$ ($x = 0.08$).

is observed above 10 K, while a loss of initial asymmetry is observed below 10 K. However, only a fast precession frequency is observed. The spectra exhibit similar behaviors which suggests the same ground state for the $x = 0.08$ and 0.15 samples. The temperature dependence of the extracted fitting

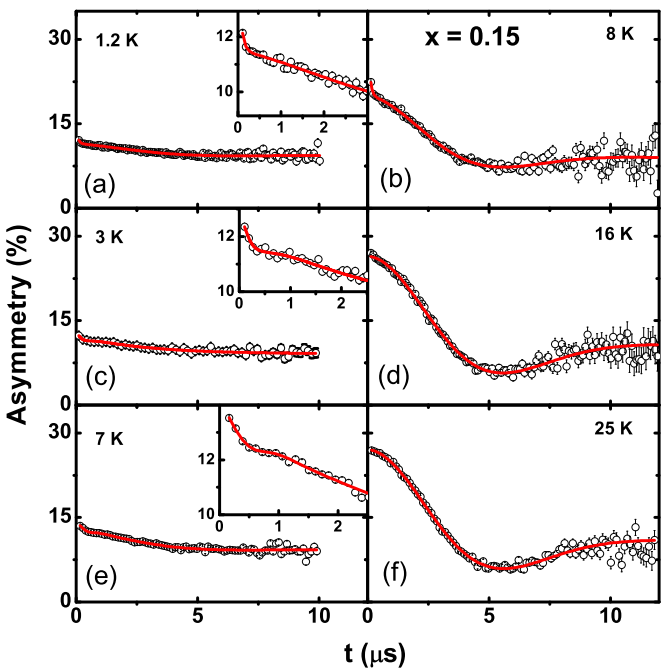

FIG. 5. (Color online) Time dependence of muon asymmetry spectra at various temperatures of $Ce(Os_{1-x}Ir_x)_2Al_{10}$ ($x = 0.15$). The solid line is a least-squares fit to the data as described in the text. Insets: The spectra in an early-time region.

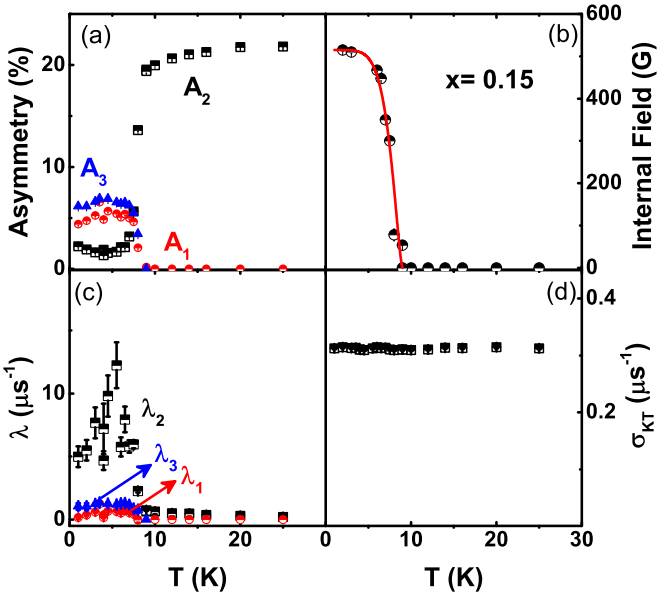

FIG. 6. (Color online) (a) The initial asymmetries A_1, A_2, and A_3, and (b) the internal field on the muon site. The solid line in (b) is fit to Eq. (3) (see text). (c),(d) The depolarization rates λ_1, λ_2, λ_3 and σ_{KT} of $Ce(Os_{1-x}Ir_x)_2Al_{10}$ ($x = 0.15$) as a function of temperature.

parameters [using Eqs. (1) and (2)] for $x = 0.15$ is shown in Figs. 6(a)–6(d).

It is interesting to compare the frequency/internal field for $x = 0.08$ and 0.15 at 2 K in order to find out how the ordered state moment increases with x. The value of the internal field observed in $x = 0.08$ and 0.15 is nearly the same, namely, 451(6) G and 510(3) G, respectively. This result shows that the ordered moment saturates faster with x (i.e., electron doping). A very similar behavior has been observed in $Ce(Ru_{1-x}Rh_x)_2Al_{10}$ [29]. In order to find out the nature of the magnetic interaction for $x = 0.08$ and 0.15, the (Ir-doped) temperature dependence of the internal field was fitted using

$$H_{\rm int}(T) = H_0\left[1 - \left(\frac{T}{T_N}\right)^{\alpha}\right]^{\beta}. \qquad (3)$$

The observed parameters are $\beta = 0.45(2)$ and 0.47(2), $H_0 = 451$ G and 510 G, $\alpha = 2.46$ and 4.4, and $T_N = 18.5(3)$ K and 8.2(2) K [see Figs. 4(b) and 6(b)] for $x = 0.08$ and 0.15, respectively. A good fit with $\beta \sim 0.45$ (or 0.47) suggests that the magnetic interactions in the electron-doped system are long-range spin-spin interactions. $\alpha > 1$ indicates complex magnetic interactions in this system [30,31].

To estimate the internal field at the muon site at low temperature, we measured the field dependence of the μ^+SR spectra. Figures 7(a)–7(c) show the effect of the applied magnetic field on the μ^+SR spectra of $Ce(Os_{0.92}Ir_{0.08})_2Al_{10}$ at (i) 5 and 15 K in the magnetic ordered state, and (ii) 30 K in the paramagnetic state. Zero-field μ^+SR spectra at 5 K reveal a strong suppression of the KT term due to a broad distribution of internal fields. On increasing the field to 100 G, the KT term disappears but the full instrumental asymmetry is not recovered until an applied field of 2500 G. This suggests that the internal fields at the muon sites are below 2500 G. For $CeOs_2Al_{10}$, we observed an internal field of less than 100 G

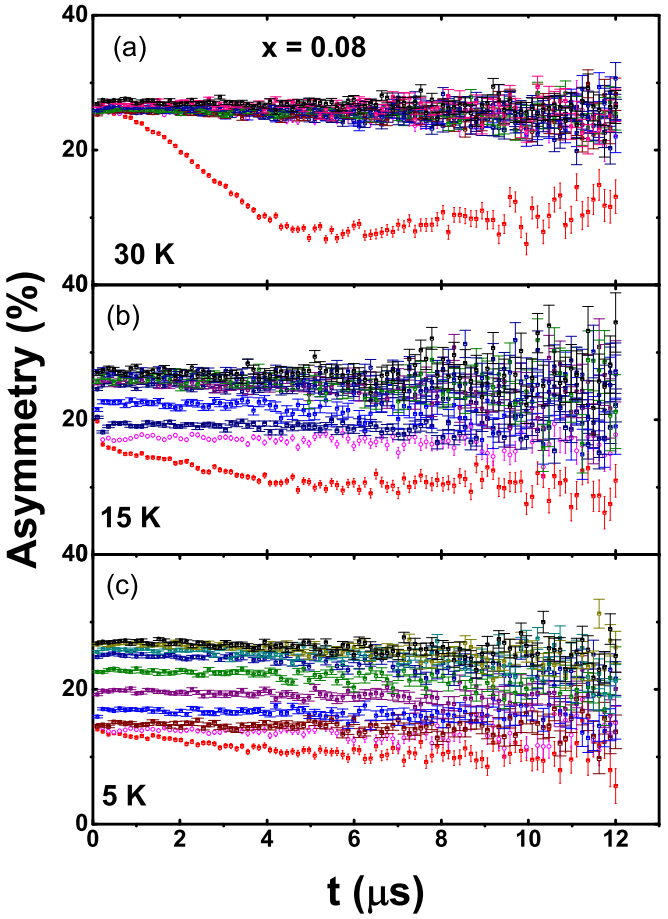

FIG. 7. (Color online) (a)–(c) The μ^+SR spectra for various applied magnetic fields (H = 0, 50, 100, 250, 500, 1000, 2000, 3000, 4000 and 4500 G) at 30, 15, and 5 K, respectively, for $Ce(Os_{1-x}Ir_x)_2Al_{10}$ ($x = 0.08$).

from field dependence μ^+SR spectra. The Kubo-Toyabe term is decoupled in a field 50 G at 30 K and the spectra are nearly time independent, as shown in Fig. 7(a).

V. INELASTIC NEUTRON SCATTERING

INS measurements on $CeOs_2Al_{10}$ clearly reveal the presence of a sharp inelastic magnetic excitation near 11 meV [as shown in Figs. 8(a) and 9(a)] between 5 and 26 K, due to the opening of a gap in the spin-excitation spectrum, which transforms into a broad response at and above 30 K [16]. A small amount of electron and hole doping results in a dramatic change in zero-field μ^+SR spectra. It is of great interest to study the electron- and hole-doped samples using inelastic neutron scattering to see how the spin gap and its Q and temperature dependence varies with doping. In this section, we report the temperature dependence of low-energy INS spectra of $Ce(Os_{1-x}Ir_x)_2Al_{10}$ ($x = 0.08$ and 0.15) and $Ce(Os_{1-y}Re_y)_2Al_{10}$ ($y = 0.03$). We have also measured the nonmagnetic phonon reference compound $LaOs_2Al_{10}$. INS investigations on CeT_2Al_{10} (T = Fe, Ru, and Os) compounds were previously reported by several groups [16,32–34].

Figures 8(a)–8(d) show the plots of the total scattering intensity (magnetic and phonon contributions), and the energy

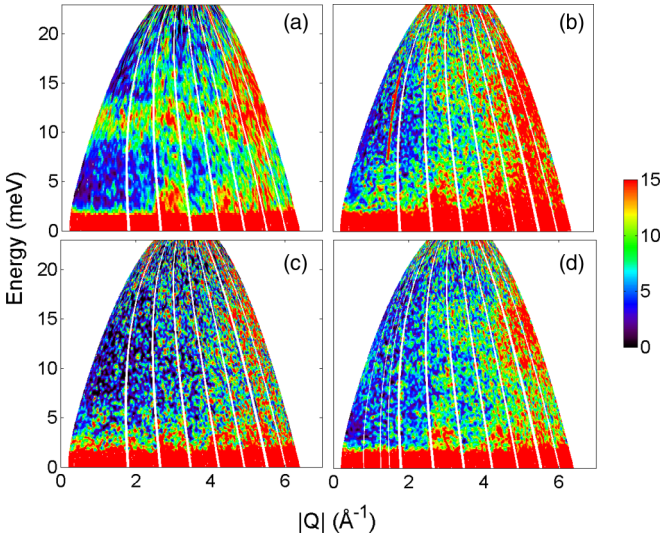

FIG. 8. (Color online) Inelastic neutron-scattering intensity of $Ce(Os_{1-x}Ir_x)_2Al_{10}$ for (a) $x = 0$, (b) $x = 0.08$, (c) $x = 0.15$, and $Ce(Os_{1-y}Re_y)_2Al_{10}$ for (d) $y = 0.03$ at 5 K, measured with respective incident energy E_i = 25 meV on the MARI spectrometer.

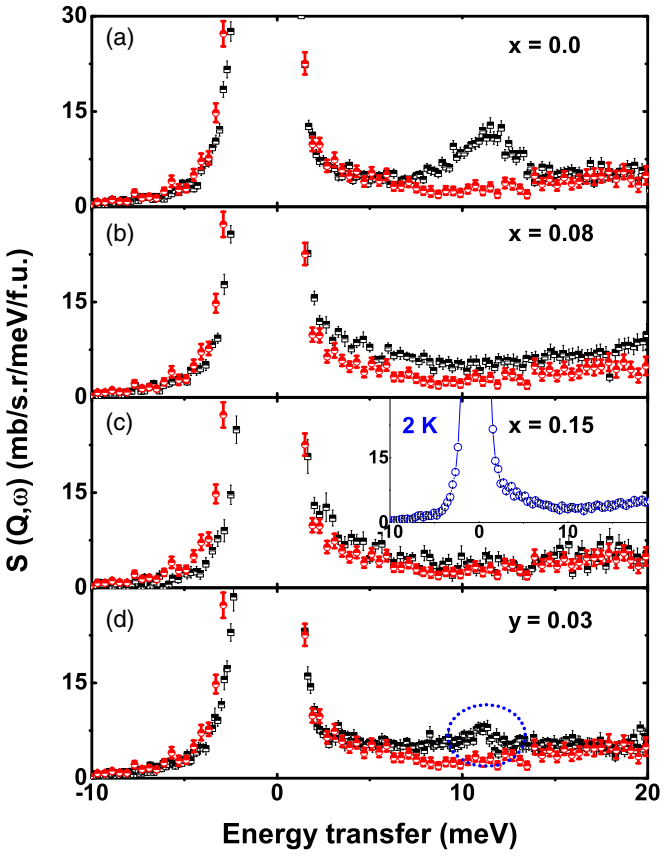

FIG. 9. (Color online) Q-integrated ($0 \leqslant Q \leqslant 2.5$ Å) intensity vs energy transfer of $Ce(Os_{1-x}Ir_x)_2Al_{10}$ for (a) $x = 0$, (b) $x = 0.08$, (c) $x = 0.15$, and $Ce(Os_{1-y}Re_y)_2Al_{10}$ for (d) $y = 0.03$ along with $LaOs_2Al_{10}$ (red circle) at 5 K, measured with respective incident energy of E_i = 25 meV. Inset: The INS spectra at 2 K for $x = 0.15$.

transfer vs momentum transfer measured at 5 K on the MARI spectrometer for $x = 0, 0.08, 0.15$ and $y = 0.03$. For an accurate estimation of magnetic scattering in the Ce compounds, we subtracted the phonons by using the data of nonmagnetic compound $LaOs_2Al_{10}$. We scaled the La data by the cross-section ratio of the Ce compounds and $LaOs_2Al_{10}$ and then subtracting from the Ce data [35]. For the undoped compound ($x = 0$), we find clear magnetic excitation or spin-gap energy of around 11 meV [16]. This value is in agreement with the spin-gap energy estimated from the exponential behavior of the observed magnetic susceptibility, specific heat, and NMR studies [36]. In the AFM ordered state for $x = 0.08$ and 0.15 samples, the excitation disappears and the response transforms into a broad quasielastic or inelastic feature, as shown in Figs. 9(b) and 9(c). On the other hand, for $y = 0.03$, we find a weak signature of magnetic excitation of around 11 meV, but the intensity is reduced compared to the pure compound. Further, for comparison, we have also shown the scattering from the nonmagnetic reference compound $LaOs_2Al_{10}$, which reveals the magnetic natures of the excitations in the Ce compounds. Since the $x = 0.15$ sample orders below 8 K, we measured the INS down to $T = 2$ K to check for any signature of a spin gap. However, it is clear from the inset of Fig. 9(c) that there is no clear sign of a spin gap.

Now we discuss the temperature dependence of the spin-gap excitation energy. Magnetic scattering at various temperatures for $x = 0.08$ and 0.15 is shown in Figs. 10 and 11. We used the ratio of the high-Q and low-Q data of $LaOs_2Al_{10}$ (i.e., ratio $= [S_{\rm high}(Q,\omega)/S_{\rm low}(Q,\omega)]_{\rm La}$) to estimate the magnetic scattering: $S_M(Q,\omega) = S_{\rm low}(Q,\omega)_{\rm Ce} - S_{\rm high}(Q,\omega)_{\rm Ce}$/ratio [35]. We have plotted the data in one-dimensional (1D) (Q integrated between 0 and 2.5 Å) energy cuts (see Figs. 10 and 11) taken from the two-dimensional (2D) plots to see the linewidth (Γ) and intensity clearly. In order to investigate the involvement of prevailing inelastic-type energy excitations, we analyzed the temperature-dependent magnetic scattering $S(Q,\omega)$ using a Lorentzian line shape [16], and fits are shown in Figs. 10 and 11 for $x = 0.08$ and 0.15. Figure 12 shows the temperature-dependent parameters estimated from the fit to the data for $x = 0.08$ and 0.15 (solid lines are quasielastic fits). The temperature dependence of the linewidth, Γ, for $x = 0.08$ and 0.15, is shown in Fig. 12(a). The quasielastic linewidth is a measure of Kondo temperature T_K (just above T_N, ideally one takes the Γ value at $T = 0$). We determined the T_K values to be 22 and 10 K for $x = 0.08$ and 0.15 compounds, respectively. The smaller value of the T_K indicates that Ce ions are nearly localized in the doped systems in contrast to the undoped parent compound. Figure 12(b) shows an estimated magnetic susceptibility for both compounds which matches well with the measured $\chi(T)$ data. Thus, the van Vleck contribution from the crystal electric-field (CEF) excited states is small at low T.

Low-energy inelastic neutron-scattering measurements on the OSIRIS and IRIS spectrometers have been carried out to further confirm whether there is any sign of quasielastic scattering present in $CeOs_2Al_{10}$ and $Ce(Os_{0.92}Ir_{0.08})_2Al_{10}$ below and above T_N. 25 and 17.5 μeV (FWHM) is the respective instrument resolution for the elastic line. It is interesting that the temperature dependence of the Q-integrated energy versus

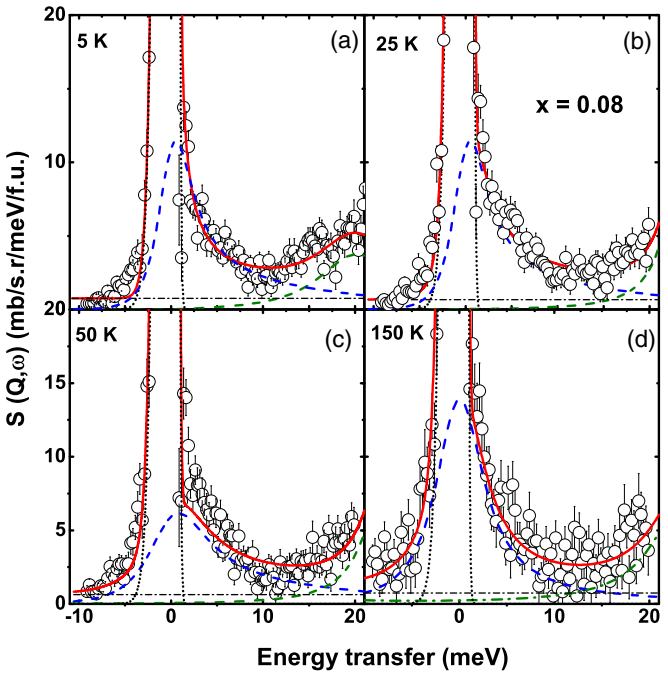

FIG. 10. (Color online) Q-integrated ($0 \leqslant Q \leqslant 2.5$ Å) intensity vs energy transfer of $Ce(Os_{1-x}Ir_x)_2Al_{10}$ ($x = 0.08$) at 5, 25, 50, and 150 K, respectively, measured with incident energy $E_i = 25$ meV. The solid line represents the fit using an inelastic peak (dash-dotted line represents the components of fit), and the dotted line represents a quasielastic peak.

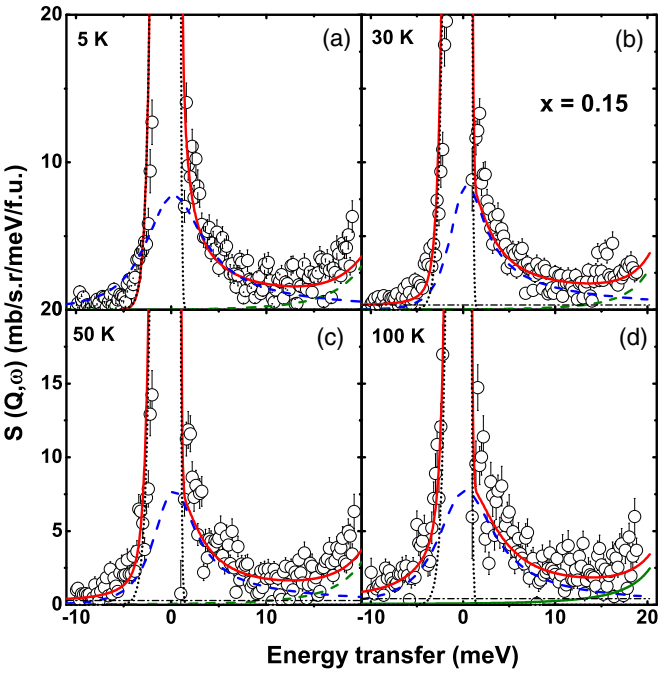

FIG. 11. (Color online) Q-integrated ($0 \leqslant Q \leqslant 2.5$ Å) intensity vs energy transfer of $Ce(Os_{1-x}Ir_x)_2Al_{10}$ ($x = 0.15$) at 5, 30, 50, and 100 K, respectively, measured with incident energy $E_i = 25$ meV. The solid line represents the fit using an inelastic peak (dash-dotted line represents the components of fit), and the dotted line represents a quasielastic peak.

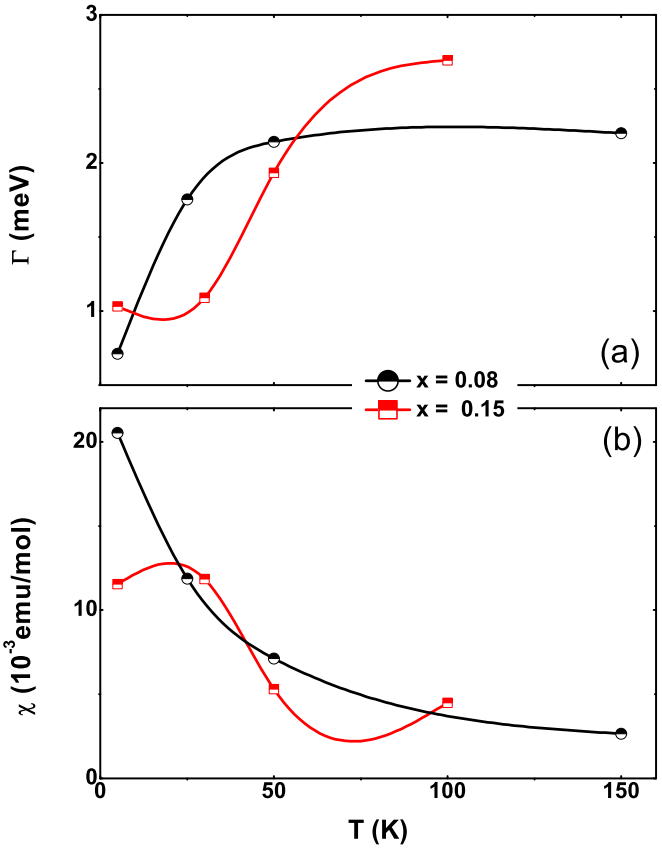

FIG. 12. (Color online) (a),(b) The variation of linewidth and susceptibility as a function of temperature obtained from fitting the magnetic scattering intensity of $Ce(Os_{1-x}Ir_x)_2Al_{10}$ ($x = 0.08$ and 0.15). Lines are guides to the eye.

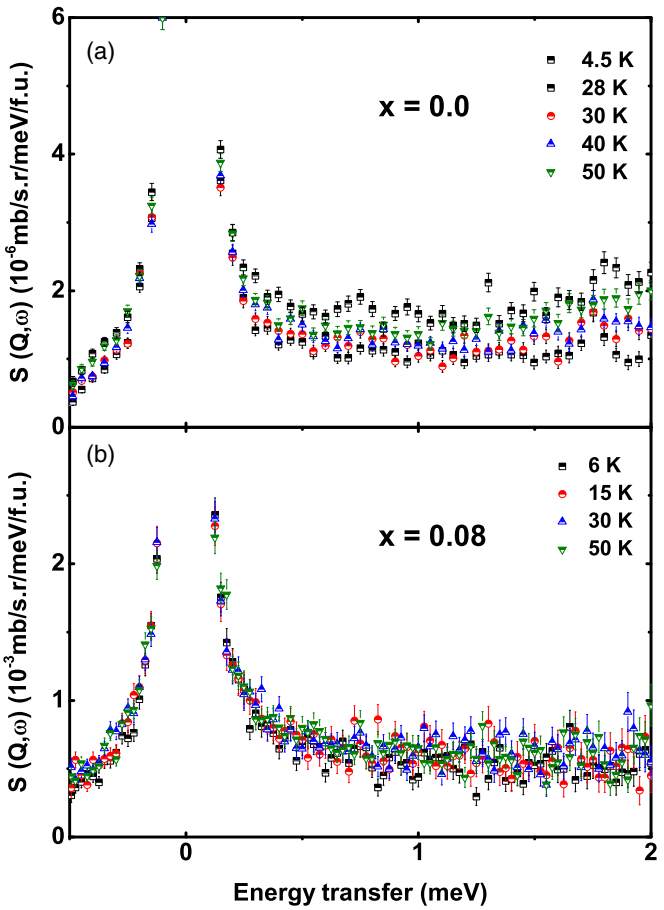

FIG. 13. (Color online) (a),(b) The $S(Q,\omega)$ for $x = 0.0$ (measured with OSIRIS spectrometer) and $x = 0.08$ (measured with IRIS spectrometer) at different temperatures, integrated over wave-vector transfer $0.5 < Q < 1.7$ Å^{-1}.

intensity data exhibits similar behavior, as shown in Figs. 13(a) and 13(b). This confirms that there is no clear signature of the quasielastic component at 4.5 K as well as no obvious development of a strong and narrow quasielastic component just above T_N. Even though for the $x = 0.08$ sample T_N is 20 K, there is no clear signature of the INS peak down to 0.4 meV, which indicates that the spin-gap or spin-wave energy scale is very small for an electron-doped system. This is also in agreement with the MARI data presented in Figs. 10 and 11, which indicate the presence of a broad quasielastic component just below T_N. If the weak quasielastic line was present just above T_N, then in both of the data sets it must be very broad and weak, which is not possible to determine on an IRIS/OSIRIS spectrometer.

VI. SUMMARY

A μ^+SR and inelastic neutron-scattering study has been performed on the caged-type compounds $Ce(Os_{1-x}Ir_x)_2Al_{10}$ ($x = 0.08$ and 0.15) and $Ce(Os_{1-y}Re_y)_2Al_{10}$ ($y = 0.03$) to understand the unusual AFM phase transition and spin-gap formation. Our μ^+SR spectra for $x = 0.08$ and 0.15 clearly reveal the presence of the long-range magnetic ordering at low temperature. One muon frequency is observed for electron-doped samples in contrast to three frequencies in the parent $CeOs_2Al_{10}$ compound. The internal field at the corresponding muon site is enhanced by about ten times by a small amount of electron doping, which supports the larger moment being along the a axis in the Ir-doped sample, as revealed by our recent neutron-diffraction experiment on $x = 0.08$. Further, nearly the same values of the internal field in the $x = 0.08$ and 0.15 samples at 2 K indicate that ordered state moments are nearly the same in both samples. This indicates the rapid saturation of the Ce moment with electron doping. A very similar effect has been observed in $Ce(Ru_{1-x}Rh_x)_2Al_{10}$ [29]. The AFM structure of $CeOs_2Al_{10}$ is not so robust and can be easily changed by very small external perturbations such as chemical doping. The important results are that a small amount of electron doping ($5d$) completely suppresses the inelastic excitation near 11 meV, which is present in the undoped compound. The main origin of the observed doping effect is the extra $5d$ electrons carried by Ir. Our study has revealed important results in the wider framework of spin-gap formation driven by $4f$ and conduction-electron hybridization. Further study of single crystals of $Ce(Os_{1-x}Ir_x)_2Al_{10}$ is highly desirable using low- as well as high-energy inelastic neutron scattering, also in the polarized mode, to confirm the disappearance of the spin gap in the electron-doped systems.

ACKNOWLEDGMENTS

We would like to thank P. Deen, D. D. Khalyavin, and W. Kockelmann for interesting discussions. D.T.A. and A.B thank the FRC of UJ and ISIS-STFC for funding support. D.T.A. and A.D.H. would like to thank CMPC-STFC, Grant No. CMPC-09108, for financial support. A.M.S. thanks the SA-NRF (Grant No. 78832) and UJ Research Committee for financial support. T.T. thanks KAKENHI (Grant No. 26400363) from JSPS.

[1] L. Degiorgi, Rev. Mod. Phys. **71**, 687 (1999).

[2] P. Wachter, in *Handbook on the Physics and Chemistry of Rare Earths*, edited by K. A. Gschneidner and L. Eyring (Elsevier Science, New York, 1994), Vol. 19.

[3] A. Amato, Rev. Mod. Phys. **69**, 1119 (1997).

[4] S. Doniach, Physica B+C (Amsterdam) **91**, 231 (1977).

[5] A. J. Millis and P. A. Lee, Phys. Rev. B **35**, 3394 (1987).

[6] A. Georges, G. Kotliar, W. Krauth, and M. J. Rozenberg, Rev. Mod. Phys. **68**, 13 (1996).

[7] P. Fulde, *Electron Correlations in Molecules and Solids*, 2nd ed. (Springer-Verlag, Berlin, 1993).

[8] A. C. Hewson, *The Kondo Problem to Heavy Fermions* (Cambridge University Press, Cambridge, 1997).

[9] P. Coleman, Phys. Rev. Lett. **59**, 1026 (1987).

[10] A. M. Awasthi, L. Degiorgi, G. Grüner, Y. Dalichaouch, and M. B. Maple, Phys. Rev. B **48**, 10692 (1993).

[11] L. Degiorgi, S. Thieme, H. R. Ott, M. Dressel, G. Grner, Y. Dalichaouch, M. B. Maple, Z. Fisk, C. Geibel, and F. Steglich, Z. Phys. B **102**, 367 (1997).

[12] D. A. Bonn, J. D. Garrett, and T. Timusk, Phys. Rev. Lett. **61**, 1305 (1988).

[13] S. Donovan, A. Schwartz, and G. Grüner, Phys. Rev. Lett. **79**, 1401 (1997).

[14] P. E. Sulewski, A. J. Sievers, M. B. Maple, M. S. Torikachvili, J. L. Smith, and Z. Fisk, Phys. Rev. B **38**, 5338 (1988).

[15] Y. Muro, K. Motoya, Y. Saiga, and T. Takabatake, J. Phys. Soc. Jpn. **78**, 083707 (2009); D. D. Khalyavin, A. D. Hillier, D. T. Adroja, A. M. Strydom, P. Manuel, L. C. Chapon, P. Peratheepan, K. Knight, P. Deen, C. Ritter, Y. Muro, and T. Takabatake, Phys. Rev. B **82**, 100405(R) (2010).

[16] D. T. Adroja, A. D. Hillier, P. P. Deen, A. M. Strydom, Y. Muro, J. Kajino, W. A. Kockelmann, T. Takabatake, V. K. Anand, J. R. Stewart, and J. Taylor, Phys. Rev. B **82**, 104405 (2010); D. T. Adroja, A. D. Hillier, Y. Muro, J. Kajino, T. Takabatake, P. Peratheepan, A. M. Strydom, P. P. Deen, F. Demmel, J. R. Stewart, J.W. Taylor, R. I. Smith, S. Ramos, and M. A. Adams, *ibid.* **87**, 224415 (2013).

[17] T. Nishioka, Y. Kawamura, T. Takesaka, R. Kobayashi, H. Kato, M. Matsumura, K. Kodama, K. Matsubayashi, and Y. Uwatoko, J. Phys. Soc. Jpn. **78**, 123705 (2009).

[18] A. M. Strydom, Physica B **404**, 2981 (2009).

[19] Y. Muro, J. Kajino, K. Umeo, K. Nishimoto, R. Tamura, and T. Takabatake, Phys. Rev. B **81**, 214401 (2010).

[20] A. Bhattacharyya, D. D. Khalyavin, D. T. Adroja, A. M. Strydom, A. D. Hiller, P. Manuel, T. Takabatake, J. W. Taylor, and C. Ritter, Phys. Rev. B **90**, 174412 (2014).

[21] S.-i. Kimura, T. Iizuka, H. Miyazaki, A. Irizawa, Y. Muro, and T. Takabatake, Phys. Rev. Lett. **106**, 056404 (2011).

[22] J. Kawabata, T. Takabatake, K. Umeo, and Y. Muro, Phys. Rev. B **89**, 094404 (2014).

[23] F. Strigari, T. Willers, Y. Muro, K. Yutani, T. Takabatake, Z. Hu, S. Agrestini, C.-Y. Kuo, Y.-Y. Chin, H.-J. Lin, T. W. Pi, C. T. Chen, E. Weschke, E. Schierle, A. Tanaka, M. W. Haverkort, L. H. Tjeng, and A. Severing, Phys. Rev. B **87**, 125119 (2013).

[24] H. Kato, R. Kobayashi, T. Takesaka, T. Nishioka, M. Matsumura, K. Kaneko, and N. Metoki, J. Phys. Soc. Jpn. **80**, 073701 (2011).

[25] D. D. Khalyavin, D. T. Adroja, P. Manuel, J. Kawabata, K. Umeo, and T. Takabatake, and A. M. Strydom, Phys. Rev. B **88**, 060403(R) (2013).

[26] D. D. Khalyavin, D. T. Adroja, A. Bhattacharyya, A. D. Hillier, P. Manuel, A. M. Strydom, J. Kawabata, and T. Takabatake, Phys. Rev. B **89**, 064422 (2014).

[27] S. Kambe, H. Chudo, Y. Takunaga, T. Koyama, H. Sakai, T. U. Ito, K. Ninomiya, W. Higemoto, T. Takesaka, T. Nishioka, and Y. Miyake, J. Phys. Soc. Jpn. **79**, 053708 (2010).

[28] H. Guo, H. Tanida, R. Kobayashi, I. Kawasaki, M. Sera, T. Nishioka, M. Matsumura, I. Watanabe, and Z. A. Xu, Phys. Rev. B **88**, 115206 (2013).

[29] R. Kobayashi, K. Kaneko, K. Saito, J.-M. Mignot, Gilles Andŕe, J. Robert, S. Wakimoto, M. Matsuda, S. Chi, Y. Haga, T. D. Matsuda, E. Yamamoto, T. Nishioka, M. Matsumura, H. Tanida, and M. Sera, J. Phys. Soc. Jpn. **83**, 104707 (2014).

[30] D. I. Khomskii, *Basic Aspects of the Quantum Theory of Solids: Order and Elementary Excitations* (Cambridge University Press, Cambridge, 2010).

[31] S. Blundell, *Magnetism in Condensed Matter*, Oxford Master Series in Condensed Matter (Oxford University Press, Oxford, 2001).

[32] D. T. Adroja, A. D. Hillier, Y. Muro, T. Takabatake, A. M. Strydom, A. Bhattacharyya, A. Daoud-Aladin, and J. W. Taylor, Phys. Scr. **88**, 068505 (2013).

[33] J.-M. Mignot, P. A. Alekseev, J. Robert, S. Petit, T. Nishioka, M. Matsumura, R. Kobayashi, H. Tanida, H. Nohara, and M. Sera, Phys. Rev. B **89**, 161103 (2014).

[34] J. Robert, J.-M. Mignot, S. Petit, P. Steffens, T. Nishioka, R. Kobayashi, M. Matsumura, H. Tanida, D. Tanaka, and M. Sera, Phys. Rev. Lett. **109**, 267208 (2012).

[35] D. T. Adroja, J.-G. Park, K. A. McEwen, N. Takeda, M. Ishikawa, and J.-Y. So, Phys. Rev. B **68**, 094425 (2003).

[36] C. S. Lue, S. H. Yang, T. H. Su, and B.-L. Young, Phys. Rev. B **82**, 195129 (2010).